LBNL-39656
UC-401

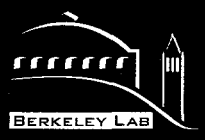

ERNEST ORLANDO LAWRENCE
BERKELEY NATIONAL LABORATORY

CONF-960807--12

Photodissociation of Ozone at 276nm by Photofragment Imaging and High Resolution Photofragment Translational Spectroscopy

D.A. Blunt and A.G. Suits
Chemical Sciences Division

November 1996
Presented at the
ACS 212th National Annual Meeting,
Orlando, FL,
August 25–30, 1996,
and to be published in
the Proceedings

LBNL-39656
UC-401

Photodissociation of Ozone at 276nm by Photofragment Imaging and High Resolution Photofragment Translational Spectroscopy

D.A. Blunt and A.G. Suits

Chemical Sciences Division
Ernest Orlando Lawrence Berkeley National Laboratory
University of California
Berkeley, California 94720

November 1996

This work was supported by the Director, Office of Energy Research, Office of Basic Energy Sciences, Chemical Sciences Division, of the U.S. Department of Energy under Contract No. DE-AC03-76SF00098.

Photodissociation of Ozone at 276nm by Photofragment Imaging and High Resolution Photofragment Translational Spectroscopy

D. A. Blunt and A. G. Suits

Chemical Sciences Division, Ernest Orlando Lawrence Berkeley National Laboratory, University of California, Berkeley, CA 94720

The photodissociation of ozone at 276nm is investigated using both state resolved ion imaging and high-resolution photofragment translational spectroscopy. Ion images from both [3+1] and [2+1] resonance enhanced multiphoton ionization of the $O(^1D)$ photofragment are reported. All images show strong evidence of $O(^1D)$ orbital alignment. Photofragment translational spectroscopy time-of-flight spectra are reported for the O_2 ($^1\Delta_g$) photofragment. Total kinetic energy release distributions determined from these spectra are generally consistent with those distributions determined from imaging data. Observed angular distributions are reported for both detection methods, pointing to some unresolved questions for ozone dissociation in this wavelength region.

The power of state resolved ion imaging to reveal sometimes subtle effects in a number of chemical processes is well established (*1*). However, there is often the lack of an overall picture of the process under investigation. Without this it can be difficult to properly interpret and indeed validate the observations. This study combines in one apparatus the imaging technique with the universal detection of high-resolution photofragment translational spectroscopy (PTS) (*2,3*). Photodissociation of ozone in the Hartley band is investigated as a test case to show that results from both detection methods are consistent. In future studies where only one method is employed for a given fragment this proof of consistency will be crucial. For example, it is theoretically possible to measure a fragment's recoil angular distribution with both imaging and PTS, however, the former method is much faster in collection time and simpler in subsequent analysis. The PTS method can have a higher resolving power in the laboratory frame, especially important where there are a number of competing channels leading to the formation of a given fragment (*4*). Additionally, there are a number of species for which ionization or excited-state formation schemes are undetermined. In this case imaging cannot be used. Overall, there is great flexibility afforded in having the two detection methods in one apparatus. We will demonstrate that the two methods are consistent for the most part and where they differ explanation is given.

We chose ozone because the photodissociation dynamics in the Hartley band have been investigated by several groups (*4-7*). At 276nm the primary channels are:

$$O_3 + h\upsilon \rightarrow O_2(^1\Delta_g) + O(^1D)$$
$$\rightarrow O_2(^3\Sigma_g^-) + O(^3P)$$

where 85-90% of fragmentation leads to singlet species (*5-7*). Total cross-section for the process is large - approximately $5x10^{-16}cm^2$ (*8*). The dissociation energy for the singlet channel is 386kJ/mol while it is only 101kJ/mol for the triplet case (*8*). Experimentally the recoil velocities of singlet photofragments are more favorable for study. There is the possibility of resolving vibrational structure in both imaging and PTS time-of-flight spectra whereas with the faster ground state fragments this would be difficult. Vibrational structure is observed in previous PTS studies of ozone near this wavelength and also in the pioneering work of Fairchild et al. (*5*).

In our experiment the molecular oxygen fragment is investigated with PTS. Higher background counts at mass-to-charge ratio 16 makes study of the $O(^1D)$ fragment more difficult, instead a newly published scheme for detecting $O(^1D)$ by [3+1] resonance enhanced multiphoton ionization (REMPI) near 276nm is employed (9). This paper presents ion images using this REMPI scheme for the first time. An existing method of detecting the $O(^1D)$ fragment, [2+1] REMPI near 205nm, is also utilized (*10*). It should be noted that with this discussion of different wavelengths the dissociation step is always with 276nm light.

Experimental

Vacuum Apparatus. Figure 1 illustrates the vacuum apparatus used for these experiments. A complete description will be given elsewhere, however a brief summary is presented here (Blunt, D.; Suits, A.G. unpublished data). The supersonic beam is formed in a rotatable chamber through a pulsed .024" diameter orifice (General Valve Corporation). Pressure in the source is typically 10^{-5}torr with a 860torr helium/ozone mixture. The chamber is pumped by a 600l/s high-throughput magnetically levitated turbomolecular pump (STP-H600C, Seiko Seiki). The mach disk of the expansion is attached to a 1mm diameter skimmer at a distance of 5mm and the beam passes into the main chamber which is held at 10^{-7}torr by a 1000l/s magnetically levitated turbomolecular pump (STP-1000, Seiko Seiki). Quartz windows on the main chamber admit the laser beam(s) on an axis perpendicular to both the molecular beam and detector axes.

Imaging Detector. For ion imaging experiments an electrode assembly consisting of three equispaced mesh plates is mounted directly in front of the source chamber. DC potentials of +700, +380 and 0V are applied to the plates and ions formed by laser/molecular beam interaction are accelerated into a field free tube leading toward the imaging detector. The detector is pumped by a 400l/s magnetically levitated turbomolecular pump (STP-400, Seiko Seiki) and the pressure is typically 10^{-9} torr during operation of the molecular beam.

Ions are detected on an enhanced 40mm diameter dual microchannel plate (MCP) Chevron-type assembly (3040FM, Galileo). A voltage of -1.9kV DC is applied to the front MCP while the other is held at ground. Electron multiplication takes place and these are accelerated toward a phosphor screen biased at +4.5kV DC. A CCD camera (512x512 16-bit, Princeton Applied Research) records the phosphor image and this is transferred to computer for storage and subsequent analysis. In addition a photomultiplier tube is positioned to allow ion time-of-flight to be recorded. The ion of interest (O^+) is selectively detected by gating the front MCP from -1.4kV to -1.9kV at the O^+ ion flight time.

PTS Detector. For PTS experiments the ion lens assembly is removed and the source rotated to the desired laboratory angle. Photofragments are admitted to the electron impact bombardment ionizer via a 4mm diameter aperture in the main chamber. Ions are formed at 100eV, selectively transmitted through a quadrupole mass spectrometer, and then detected with a standard Daly ion detector (*2*). The detector region is pumped by

two 400l/s magnetically levitated turbomolecular pumps (STP-400, Seiko Seiki) and a third pump of the same type evacuates a differential region between the main chamber and ionization region. With a liquid nitrogen cooled copper shield around the ionizer base pressures of $7x10^{-11}$ torr are achieved. In addition, a copper plate is mounted in front of the source chamber and maintained at 10K with a heat exchanger (HC-2, Air Products), resulting in low background count rates. The signal from the Daly ion detector is connected to a computer controlled multichannel scaler (Turbo-MCS, EG&G Ortec). Pulsing the nozzle at 40Hz allows laser-on/laser-off shot-by-shot subtraction and this greatly reduces the presence of direct beam signal at small laboratory angles (*4*).

Ozone Generation. Ozone is generated by discharge through an oxygen flow and is subsequently trapped on silica gel at -80°C. For experiments the trap is warmed to -40°C and 800torr ultra-high purity helium is passed over the gel. All tubing is Teflon with stainless steel fittings. A total nozzle backing pressure of 860torr is achieved. Ozone is seen to remain almost constant during the course of measurements. The velocity distribution of the molecular beam is determined by laser-induced hole burning of the ozone at zero degrees. Least squares fitting of the distribution $f(v) \propto v^2\exp[-(v-v_o)/\alpha^2]$ gives values of v_o = 1309m/s and α = 105m/s.

Laser Configuration. A single laser setup is used for both the PTS and single-color imaging experiments. The second harmonic of a seeded Nd:YAG laser (GCR-5, Spectra Physics) pumps a dye laser at 10Hz (PDL-1, Quanta-Ray). With 700mJ/pulse we obtain 200mJ/pulse of 552nm light. This light is doubled with a KD*P crystal in a wavelength extender (WEX-1, Quanta-Ray). Up to 25mJ/pulse of linearly polarized light is available at 276nm. For measurement of vibrational state distributions via PTS, the light is passed through a single fresnel rhomb at 45 degrees to produce circularly polarized light. Where focusing is required (for the [3+1] REMPI) a 25cm focal length fused silica lens is inserted just prior to the beam entering the vacuum apparatus. The dye laser output wavelength is adjusted under computer control to facilitate scanning the REMPI line Doppler width during imaging experiments.

For the [2+1] REMPI measurements (at ~205nm) a two-color scheme is used. The dissociation laser pulse (276nm) is formed via the same scheme described above, however the pump laser is an unseeded Nd:YAG laser (DCR-2A, Quanta-Ray) capable of 500mJ/pulse at 532nm. Up to 10mJ/pulse of 276nm light is available for the dissociation. This is weakly focused at the interaction region with a 47.5cm focal length fused silica lens.

The 205nm light for the [2+1] REMPI is generated using the GCR-5/PDL-1 combination where the dye is Sulphorhodamine 640, giving 190mJ/pulse of 615nm light. This is passed through a double fresnel rhomb and 'UV' half-wave plate before being doubled with a BBO crystal. The remaining 615nm light is mixed with the 307nm light in another BBO crystal to produce 100μJ/pulse of vertically polarized 205nm light. A Pellin-Broca prism separates the 205nm beam and this is then tightly focused at the interaction region with a 10cm focal length fused silica lens.

The purpose of the polarizing elements prior to doubling are to produce enough red light in the correct polarization for both doubling and mixing stages. As in the single laser experiment, dye laser output wavelength is controlled by computer.

Results and Discussion

The primary concern of this paper is to compare the data obtained by ion imaging with PTS time-of-flight spectra. There are two convenient schemes for detecting $O(^1D)$ via resonance enhanced multiphoton ionization (REMPI). Firstly, two resonances near 205nm corresponding to [2+1] processes and, more recently discovered, five

resonances near 276nm which are [3+1] processes. We have measured ion images at each of these lines, but for this paper we will restrict our attention to three representative data sets.

PTS. Time-of-flight spectra of the O_2 photofragment are recorded at two laboratory wavelengths (20 and 30 degrees) for each of five dissociation wavelengths near 276nm. In addition, each spectrum is recorded once using circularly polarized light and then again with linearly polarized light. From these measurements the total kinetic energy release and center-of-mass angular recoil distributions are determined. The principal reason for performing the PTS experiments at five different wavelengths is to allow comparison with single-color ion imaging data where the detection is via one of the five $O(^1D)$ [3+1] REMPI lines near 276nm. Comparison with the imaging data is discussed later in this section. A previous investigation of ozone photodissociation in this region of the Hartley band reports rapid variation of the O_2 vibrational state distribution with wavelength, however over the narrow range of wavelengths investigated here it is not possible to draw such a conclusion (*7*).

Results for two wavelengths using circularly polarized light are presented in Figure 2. In this experimental arrangement the use of circularly polarized light results in isotropic fragment angular recoil direction in the detector-molecular beam plane. Determining the total kinetic energy release distribution, $P(E)$, is simplified without this possible (and likely) anisotropy. The energy available after dissociation for fragment degrees of freedom is no more than 46kJ/mol. Only the lowest three vibrational levels of O_2 are accessible. Peaks corresponding to these levels are clearly resolved in the PTS spectra at 20 degrees. At a wider angle only v = 0 and v = 1 are observed since that angle is outside the maximum velocity circle of v = 2 fragments. Fitting of the data sets is performed by forward convolution of a trial $P(E)$ with experimental parameters (*11*). This trial distribution is refined until good agreement between experimental and calculated laboratory TOF spectra is achieved.

The partitioning of available energy into the three vibrational levels is determined from these $P(E)$ by calculating the relative contributions of each component to the time-of-flight spectra at 20 degrees. Our findings for all five wavelengths are shown in Table I. Data for each wavelength is collected over a single day. Variation of the v = 1 / v = 0 and v = 2 / v = 0 ratios with wavelength may be in part due to varying initial source conditions each day, yet as noted previously, the ozone signal varied little over the course of a given day. The average value for v = 1 / v = 0 (0.63) is higher than the 0.5 determined by Thelen et al. (*7*). This discrepancy is possibly due to the different source conditions employed in their experiments. Thelen et al. find a mean flow velocity of 1705m/s and a half-height width of 55m/s, suggesting that the ozone was rotationally cooler than in our setup. With a different set of initial states it is quite possible that a different O_2 vibrational state distribution would result. Average total kinetic energy release for each vibrational level is consistent with previous measurements at 266 and 283nm and is discussed later in this section (*5,6*).

Table I. Vibrational State Distributions for the $O_2(^1\Delta_g)$ Photofragment

Wavelength (nm)	v = 1 / v = 0	v = 2 / v = 0
276.53	0.73	0.41
276.55	0.64	0.33
276.66	0.58	0.20
276.70	0.60	0.39
276.75	0.58	0.33

Product recoil angular distributions are determined by convolving the $P(E)$ from above with a trial distribution and fitting this to time-of-flight spectra recorded with linearly polarized light. The trial distribution is of the form

$$I(\theta) = N\left[1 + \beta P_2\left(\cos^2\theta\right)\right] \qquad (1)$$

where P_2 is the second Legendre polynomial, β is the anisotropy parameter, and N the usual normalization constant. A value of 0.71(0.17) is obtained for β. This value for β is significantly lower than the 1.6(0.2) reported by Thelen et al. (*7*). The asymptotic limit for β assuming equilibrium geometry for ozone is 1.18 (*5*). Using this equilibrium geometry may be incorrect since it has been shown that bending motion is important in the ozone decay and thus a different geometry would be a better choice (*4*). However, since the upper state is more strongly bent than the ground state, the expected asymptotic value for β is lower than the 1.18 determined from the equilibrium geometry, rather than the higher value (1.60) observed by Thelen et al. Another possible interpretation is the role of the parent rotation, cited by Thelen et al. to account for the difference between their result and those of Fairchild et al. in an effusive beam. At any rate this remains one of the interesting unanswered questions.

Ion Imaging. Figure 3 presents the two dimensional projections of the three dimensional ion sphere for three detection wavelengths, 276.53, 276.55 and 205.47nm. This is the first report of images recorded using the [3+1] REMPI scheme near 276nm. Collection times for the [3+1] REMPI images are typically one hour since not only is the ion flux low, but the Doppler width of the transitions must also be scanned. [2+1] REMPI images were collected in just 15 minutes. However, even a one hour collection time is much less than would be required to collect PTS time-of-flight spectra over the same center-of-mass angular range.

There are three obvious features in these images and one perhaps not so clear until the data is transformed into the total kinetic energy release distribution. Three rings are visible in each image. Working outward from the center of the image these correspond to the vibrational levels v = 2, 1, and 0, respectively, of the O_2 fragment. Secondly, the observed angular distributions for the three images are remarkably different. At 276.55nm there is a striking lack of intensity at 0 and 180 degrees for the v = 0 and 1 states. The 205.47nm image shows a truncated distribution when compared to the 276nm images. Finally, there is a variation in the angular distribution with recoil velocity. The first two effects arise from alignment of the $O(^1D)$ orbital, yielding an anisotropic distribution of the REMPI transition dipole moment in the center-of-mass frame. Analysis of this orbital alignment, or v-J vector correlation, will be reported in a future publication. However, recoil velocity information is available even prior to a detailed analysis of the v-J correlation.

To extract the total kinetic energy release distribution a two dimensional slice of the three dimensional ion sphere is reconstructed from the two dimensional projection by an inverse Abel transform (*12*). Figure 4 presents the total $P(E)$ for two of the images and also that obtained from PTS data. The three vibrational state components are present and importantly the energies of each component are matched between PTS and imaging data. Vector correlation effects in the imaging experiment prevent direct quantitative comparison of the relative contributions of each component. Figure 5 illustrates the variation of observed angular distribution between imaging and PTS data sets. The angular distribution for PTS data is calculated using $\beta = 0.71$ and equation 1.

Conclusion

Whilst there are still unresolved questions about the dissociation dynamics of ozone in this wavelength region, the combined techniques of ion imaging and PTS provide a rich source of information. We have presented PTS time-of-flight spectra that are largely consistent with previous investigations. The first ion images of the $O(^1D)$ fragment detected by [3+1] REMPI near 276nm are reported. In addition, images from detection near 205nm are recorded. All images show strong evidence of orbital alignment. Total kinetic energy release distributions from both detection methods are determined and the positions of the three vibrational state components are equivalent. An angular distribution for the dissociating fragments is calculated and shown to be in general agreement with some previous measurements. Vector correlation effects are observed in all $O(^1D)$ ion images preventing the determination of an angular distribution, however, future analysis of these effects is planned and will allow the angular information to be extracted as well as providing detailed insight into nonadiabatic processes in the dissociation dynamics. Finally, we have shown the advantages of an apparatus possessing these two complementary detection methods.

Acknowledgments

This work was supported by the Director, Office of Energy Research, Office of Basic Energy Sciences, Chemical Sciences Division of the U.S. Department of Energy under Contract No. DE-AC03-76SF00098.

Literature Cited

1. Houston, P.L. *J. Phys. Chem.* **1996**, 100, 12757.
2. Lee, Y.T.; McDonald, J.D.; LeBreton, P.R.; Herschbach, D.R. *Rev. Sci. Instrum.* **1969**, 40, 1402.
3. Wodtke, A.M.; Lee, Y.T. *J. Phys. Chem.* **1985**, 89, 4744.
4. Stranges, D.; Yang, X.; Chesko, J.D.; Suits, A.G. *J. Chem. Phys.* **1995**, 102(15), 6067.
5. Fairchild, C.E.; Stone, E.J.; Lawrence, G.M. *J. Chem. Phys.* **1978**, 69, 3632.
6. Sparks, R.K.; Carlson, L.R.; Shobatake, K.; Kowalczyk, M.L.; Lee, Y.T. *J. Chem. Phys.* **1980**, 72(2), 1401.
7. Thelen, M.-A.; Gejo, T.; Harrison, J.A.; Huber, J.R. *J. Chem. Phys.* **1995**, 103(18), 7946.
8. Okabe, H. *Photochemistry of Small Molecules*; Wiley: New York, NY, 1985.
9. Richter, R.C.; Hynes, A.J. *J. Phys. Chem.* **1996**, 100(20), 8061.
10. Pratt, S.T.; Dehmer, P.M.; Dehmer, J.L. *Phys. Rev. A* **1991**, 43(1), 282.
11. Zhao, X.; Nathanson, G.M.; Lee, Y.T. *Acta Physico-Chimica Sinica* **1992**, 8, 1.
12. Hansen, E.W.; Law, P.-L. *J. Opt. Soc. Am. A* **1985**, 2(4), 510.

Figure 1. Experimental apparatus.

Figure 2. PTS time-of-flight data: a) 276.53nm 20°, b) 276.53nm 30°, c) 276.55nm 20°, d) 276.55nm 30°.

Figure 3. Ion images from REMPI of $O(^1D)$ photofragment. From left to right, 276.53, 276.55, and 205.47nm.

Figure 4. Total kinetic energy release distributions with detection at indicated wavelength.

Figure 5. Photofragment recoil angular distributions with detection at indicated wavelength (calculated plot is based on PTS data - see text).

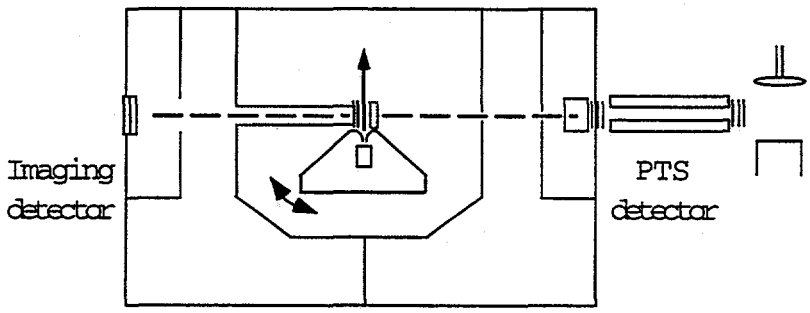
Imaging
detector
PTS
detector

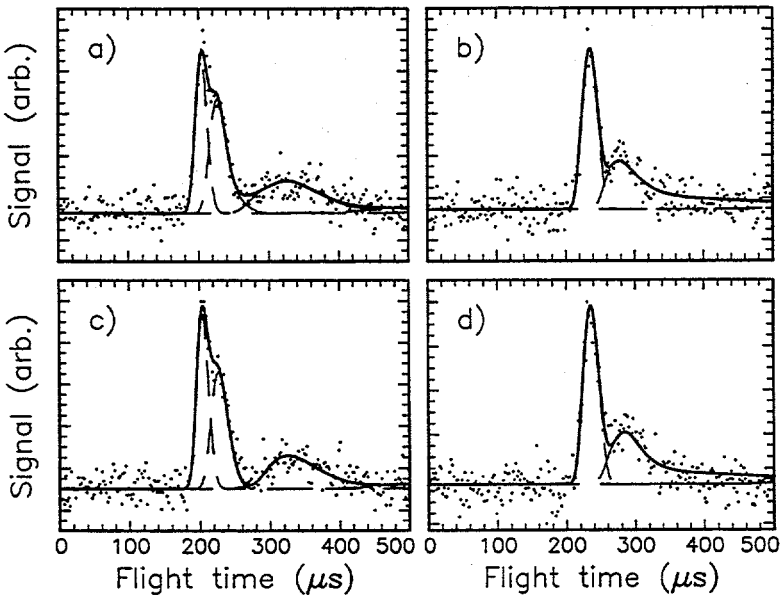
a)
b)
c)
d)
Signal (arb.)
Signal (arb.)
0
100
200
300
400
500
Flight time (μs)
Flight time (μs)

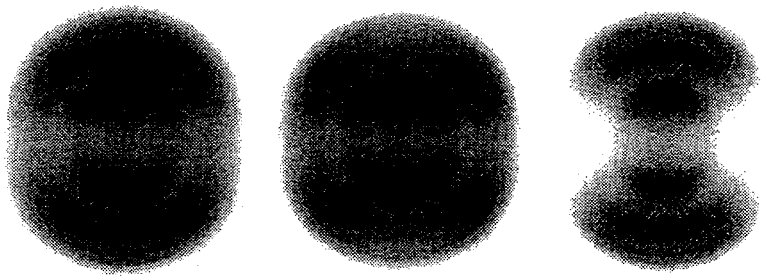

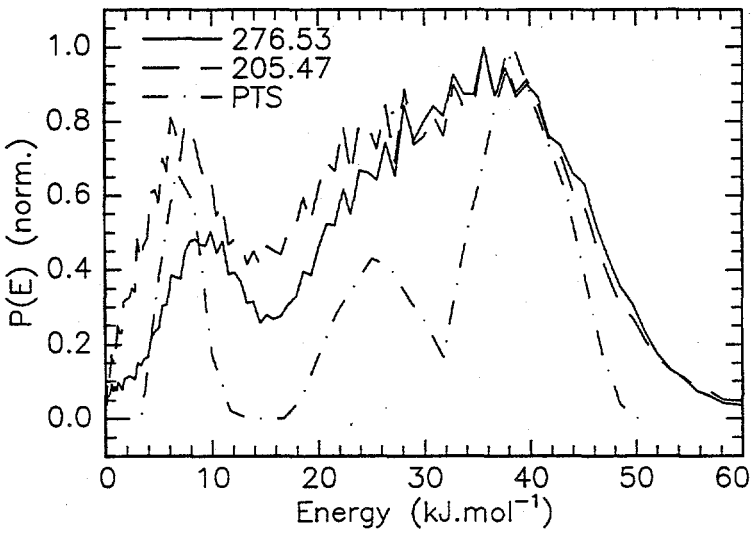
276.53
205.47
PTS
P(E) (norm.)
1.0
0.8
0.6
0.4
0.2
0.0
0
10
20
30
40
50
60
Energy (kJ.mol^{-1})

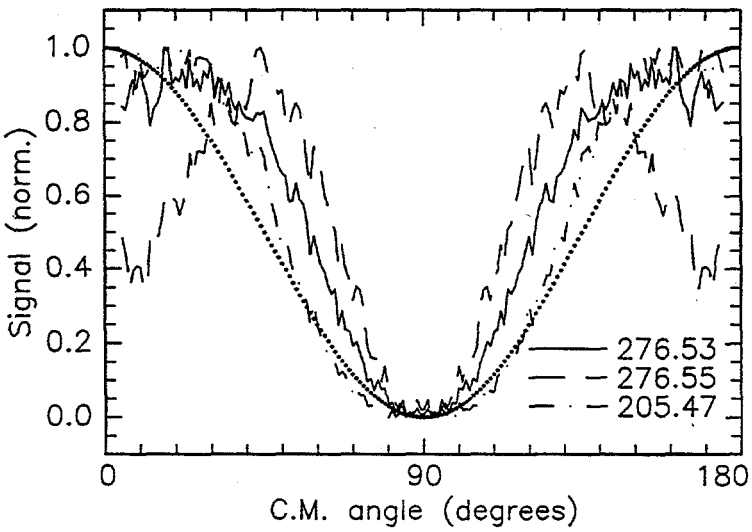
1.0
0.8
0.6
0.4
0.2
0.0
Signal (norm.)
0
90
180
C.M. angle (degrees)
276.53
276.55
205.47